Journal of Optimization in Industrial Engineering,
Vol.15, Issue 1, Winter & Spring 2022, 243-260
DOI:10.22094/JOIE.2021.1937743.1886

Research Article

Multi-objective Optimization of Turning of Titanium Alloy Under Minimum Quantity Lubrication

Satish Chinchanikar [a,*], Jitendra Kumar Katiyar [b], Omkar Manav [a]

[a] *Department of Mechanical Engineering, Vishwakarma Institute of Information Technology, Pue- 411048, India*
[b] *Department of Mechanical Engineering, SRM Institute of Science and Technology, Chennai, India*

Received 25 September 2021; Revised 20 November 2021; Accepted 05 December 2021

Abstract

In the present study, the machining performance of titanium grade-1 alloy is evaluated in terms of resultant cutting force, machined surface roughness, and material removal rate (MRR) through a multi-objective optimization approach. Turning experiments were performed with CVD-coated TiCN-Al2O3 carbide inserts using vegetable oil-based nanofluid under minimum quantity lubrication. The nanofluid was prepared using coconut oil as a base fluid mixed with boron nitride (hBN) nanoparticles. Experiments were performed by varying the cutting speed, feed, depth of cut, and nanoparticles concentration in a base fluid. The Desirability Function Approach (DFA), a Technique for Order of Preference by Similarity to Ideal Solution (TOPSIS), Grey Relational Analysis (GRA), and Non-dominated Sorting Genetic Algorithm (NSGA-II) are used to optimize the machining performance. The optimized solutions from different optimization techniques are observed in better agreement. The results show optimum performance at the higher cutting speed, higher depth of cut, lower feed, and lower concentration of nanoparticles. Lowest values for resultant force and surface roughness of 387 N and 0.47 µm, respectively, and maximum MRR of 9375 mm3/min could be obtained using the cutting speed, feed, depth of cut, and nanoparticles concentration of 125 m/min, 0.1 mm/rev, 0.75 mm, and 0.3%, respectively. However, little compromising the surface roughness to a higher value of 0.83 µm with almost the same resultant force, the higher MRR of 15000 mm3/min could be obtained using higher cutting parameters. It has been observed that the resultant force and surface roughness are significantly affected by the depth of cut and feed, respectively. However, the concentration of nanoparticles has been observed to have a lower prominent effect on the surface roughness and resultant force.

Keywords: Titanium alloy; Machining; Nanofluid MQL; Grey Relational analysis; TOPSIS; NSGA-II

1. Introduction

Titanium machining is one of the ever-growing problems due to its low thermal conductivity, modulus of elasticity, and work hardening characteristics. Titanium grade-1 alloy has a wide range of applications, especially in the marine and aerospace fields. However, achieving sustainable machining of these alloys considering economic, technical, and environmental requirements is widely researched, being difficult-to-cut material. The selection of process parameters to obtain optimum machining efficiency is very crucial for machining titanium alloys.

In machining, plastic deformation of the workpiece material at a higher strain rate causes heat generation at the cutting zone. This generated heat has a detrimental effect on the overall machining performance. The cutting fluid carries away the generated heat and assist in improving the machining economics. However, the increasing environmental and health regulations put some limits on the use of conventional cutting fluids. Further, the cost associated with the cutting fluids and their disposal after use add around 16-20% to the total production cost. Therefore, researchers have attempted machining using minimum quantity lubrication (MQL) (Dhar et al., 2007).

MQL is considered as a trade-off between the benefits and drawbacks of dry cutting and machining with ample soluble oil. MQL imparted lubricating and cooling effects that enhanced the tool life against machining under dry conditions (Liu et al., 2013). A group of researchers (Kishawy et al., 2005; Sharma et al., 2019; Maruda et al., 2017; Chinchanikar and Choudhury, 2015) observed that the machining under MQL lowered the cutting forces and improved the surface finish and tool life. Attempts have also been made to optimize MQL parameters (pressure, flow rate, type of fluid, stand-off distance, etc.) for better machining performance against machining with conventional cutting fluid (Leppert, 2011).

However, contradictory results are reported about MQL machining performance at high-speed machining (Dhar et al., 2006; Kang et al., 2008; Kumar and Ramamoorthy, 2007). It is reported ineffective cooling at high-speed machining as coolant finds it difficult to reach the cutting zone. On the other hand, researchers observed better machining performance with synthetic and vegetable oils mixed with macro/micro-sized solid particles. This mixed type of cutting fluid provided better heat transfer capacity and better lubricity (Chinchanikar et al., 2020). However,

*Corresponding author Email address: satish.chinchanikar@viit.ac.in

clogging and stability issues of micro-sized particles are reported in MQL machining (Das et al., 2006).

From the last decade, nanoparticle-assisted MQL machining made revolutionary changes in manufacturing due to its unique and enhanced properties (Aitken et al., 2006). Researchers have attempted MQL machining using a cutting fluid blended with the different nanoparticles. Thermophysical, tribological, and wetting characteristics of cutting fluids are improved by the addition of nanoparticles in base oil (Kumar et al., 2012; Chinchanikar et al., 2021). Krishna et al. (2010) investigated the temperature at the cutting zone, flank wear, and machined surface temperature during machining using nanofluids. The nanofluids were obtained by mixing solid boric acid nanoparticles with varying concentrations in the coconut oil and SAE 40 oil, respectively. Their study observed lower tool wear, lower temperature, and better surface finish due to the formation of interfacial film at the work-tool interface.

Sharma et al. (2015) reviewed nanoparticles blended cutting fluid. Their study found enhancement in the heat removal capacity from the cutting zone and improved tool life with the blended cutting fluids. A group of researchers prepared the nanofluid by mixing MoS_2 in a base oil for enhancing the tribological performance and hence the machining performance (Rahmati et al., 2014; Sharma et al., 2017). Gupta et al. (2016) investigated the effect of Aluminium oxide (Al_2O_3), Molybdenum disulphide (MoS_2), and graphite nanofluids on the machining of widely used titanium grade-2 alloy. Their study observed that graphite nanofluids significantly enhanced the machining performance by reducing the cutting force, temperature, tool wear, and surface roughness compared to the other nanofluids.

Katta et al. (2018) investigated the machining performance of Ti-6Al-4V alloy with soya bean oil mixed with graphene nanoparticles. They found a reduction in flank wear. Hegab et al. (2018) found that the Ecolubric E200 based multi-walled carbon nanotube (MWCNT) type nanofluid reduced the tool wear and power consumption by 45% and 11.5%, respectively while machining Ti-6Al-4V under MQL. Anandan et al. (2020) also observed a reduction in flank wear, surface roughness, cutting temperature, cutting forces by 60%, 26%, 34%, and 18%, respectively, while using silver nanofluid in turning titanium grade-2 alloy compared to flood lubrication.

Gaurav et al. (2020) evaluated the lubrication performance of MoS_2 nanoparticles in two different types of oils, jojoba (vegetable) and LRT30 (mineral oil), during MQL turning of Ti-6Al-4V alloy. They found that the jojoba-based MoS_2 nanofluid with MQL significantly enhances the machining performance compared to mineral oil-based cutting fluids.

Jamil et al. (2020) performed machining of Ti-6Al-4V using blaser-distilled water-based Copper oxide- multi-walled carbon nanotube (CuO-MWCNT) hybrid nanofluid under MQL. Their study observed clean machining with hybrid nanofluid as compared to carbon dioxide (CO_2) snow with a significant reduction in tool wear, power, surface roughness, and cutting temperature. Singh et al. (2021) performed the MQL assisted machining of titanium grade-5 alloy using coconut based-oil with graphite/talc nanoparticles. Their study observed that the concentration of nanoparticles prominently affects machining performance.

Kosaraju and Anne (2013) investigated the effects of process parameters such as speed, feed, depth of cut and back rake angle on cutting force and surface roughness during turning of Ti-6Al-4V using PVD-TiAlN coated carbide inserts. Their experimental study observed an increase in the cutting force with the increase in depth of cut and feed and a decrease in the cutting force with the increase in speed and back rake angle. However, surface roughness was observed as decreasing with the increase in speed and back rake angle and increased with the depth of cut and speed.

A group of researchers attempted optimization studies using different techniques (Chinchanikar and Choudhury, 2013; Kalyon et al., 2018; Kumar et al., 2018). Li et al. (2019) optimized the type of insert, feed rate, and depth of cut during turning of Ti-6Al-4V. The major performance indexes were radial thrust, cutting power, and coefficient of friction at the chip-tool interface. Grey Relational Analysis (GRA) with kernel principal component analysis (KPCA) was used to obtain the kernel grey relational grade (KGRG) and optimal process parameters. Their experimental study found that the depth of cut had the most significant effect, followed by the feed rate and type of insert. Their study observed better agreement between the experimental and predicted results with the hybrid GRA and principal component analysis (PCA) method than the traditional GRA technique.

From the literature review, it has been observed that the researchers mostly attempted machining using graphite, graphene, MWCNT, MoS_2, etc., nanoparticles mixed with vegetable-based, mineral-based oils, or water-based oils. However, nanofluid becomes black with the addition of these nanoparticles, which is mostly not preferred in manufacturing (Boyer and Briggs, 2005). Hence, attempts are being made to explore the most efficient nanofluids under MQL for the machining of titanium alloys. The preferred nanofluids must address the higher chemical affinity of the titanium alloys with other materials and low thermal conductivity (Varote and Joshi, 2017).

Continuing efforts are being made to develop nanofluids that are visible in white colour and eliminate the adhesion between the tool and the workpiece. Further, it has been observed that very few studies reported on the investigation and optimization of the machining performance of titanium grade-1 alloy using vegetable-based nanofluid under MQL. Mostly, coconut oil and sunflower oil are mostly preferred vegetable oils while machining of high temperature alloys. However, almost no studies made using coconut oil-based hexagonal boron nitride (hBN) nanofluid while machining of titanium alloy.

With this view, in the present study, the machining performance of titanium grade-1 alloy was evaluated using vegetable oil-based nanofluid under minimum

quantity lubrication. The turning performance in terms of resultant cutting force, machined surface roughness, and material removal rate was evaluated using a multi-objective optimization approach. The nanofluid was prepared using coconut oil as a base fluid mixed with hexagonal boron nitride (hBN) nanoparticles. Experiments were performed by varying the cutting speed, feed, depth of cut, and nanoparticles concentration in a base fluid. Empirical equations are developed for understanding the effect of process parameters on machining performance. The machining performance is optimized using the Desirability Function Approach (DFA), a Technique for Order of Preference by Similarity to Ideal Solution (TOPSIS), Grey Relational Analysis (GRA), and a Non-dominated Sorting Genetic Algorithm (NSGA-II) to confirm the accuracy of the results. Finally, conclusions with the scope for future work are discussed.

2. Experimental Design

Titanium grade-1 alloy is the first of four commercially pure titanium grades. It has excellent corrosion resistance and high impact toughness. Grade-1 is the material of choice for chemical processing, chlorate manufacturing, dimensionally stable anodes, medical industry, marine industry, automotive parts, airframe structure, deep drawing applications, and heat exchanger parts. It consists of 0.20% of Fe and almost 99% of titanium and all other composites. The chemical composition, physical properties, and mechanical properties of this alloy are shown in Tables 1 and 2, respectively.

Table 1.
Composition of titanium alloy (Grade-1)

Elements	Fe	O_2	C	N_2	H_2	Residuals	Ti
% Content	0.20	0.18	0.08	0.03	0.015	0.10-0.40	Balance

Table 2.
Mechanical and physical properties of grade-1 titanium alloy

Density	4.51 g/cm^3
Mean coefficient of thermal expansion	8.6 µm/m °C (20 – 100 °C)
Thermal conductivity	16 (W/m K)
Modulus of elasticity	105 – 120 kN/mm²
Melting point	1670° C
Tensile strength (MPa)	240
Yield strength, 0.2% offset (MPa)	170
Elongation (%)	24
Reduction of area (%)	30

Turning operations were performed at varying cutting speeds, feed, depth of cut, and concentration of hBN nanoparticles in the base fluid. The workpiece used was titanium grade-1 with a diameter of 25 mm and a length of 305 mm. A left-hand side cutting tool holder of size 20 by 20 mm with a carbide insert was used. The cutting insert used was a 6-point cutting tool (Triangular geometry). The CVD-coated TiCN-Al2O3 carbide inserts with the ISO designation as TNMG 160404EN-TF was used referring to the manufacturer's recommendation for machining the titanium grade-1. The tool holder used with the ISO designation as DTJNL2020K16. The tool holder and cutting insert geometries used in the present study are shown in Figures 1(a) and (b), respectively. A multilayer coating used was having an average thickness of 18.5 µm, a grain size of 1-2 µm, and a hardness of 1550 HV. The specifications of the tool holder and a cutting insert used in the present study are depicted in Tables 3 and 4, respectively.

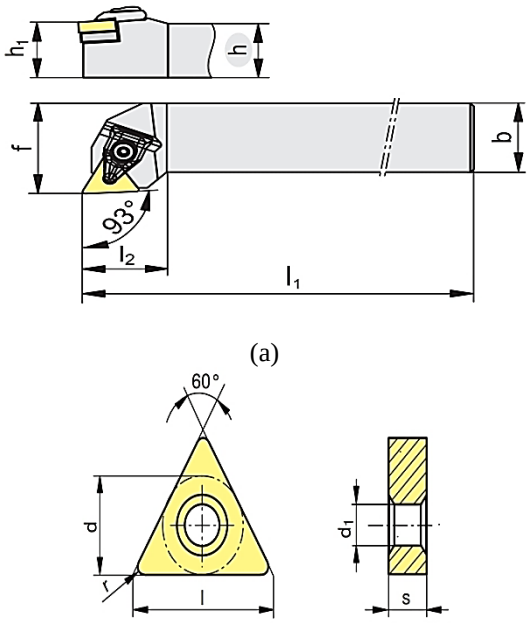

Fig. 1. (a) Tool holder geometry, (b) Cutting insert geometry

Table 3.
Specifications of tool holder

h (mm)	Type	h_1 (mm)	b (mm)	l_1 (mm)	l_2 (mm)	f (mm)
31.75	DTJNL2020K16 left-handed	31.75	31.75	152.4	31.75	38.1

Table 4.
Specifications of a cutting insert

Type	ISO version	Sub type	d (mm)	l (mm)	s (mm)	r (mm)	d1 (mm)
-TF	TNMG16404 EN-TF	CTCP115	9.525	16.51	4.7498	0.4064	3.81

The machining performance of titanium grade-1 alloy was evaluated using vegetable-based nanofluid under MQL. The nanofluid was prepared using coconut oil as a base fluid mixed with hBN nanoparticles with a size of 100-200 nm. Experiments were performed on lathe varying cutting speed, feed, depth of cut, and nanoparticles concentration in a base fluid. The process parameters were selected based on the literature review, tool manufacturer's recommendation, and pilot experiments. The different levels of cutting speed, feed, depth of cut,

and concentration of hBN nanoparticles used in the present study is as shown in Table 5.

Table 5.
Levels of process parameters

Parameters	Levels
Cutting speed (*V*) (m/min)	35, 90, 125
Feed (*f*) (mm/rev)	0.1, 0.16, 0.2
Depth of cut (*d*) (mm)	0.1, 0.5, 0.75
Nanoparticle's concentration (*C*) (%)	0.25, 0.5, 0.75

Total 27 experiments were performed at different combinations of cutting speeds, feed, depth of cut, and nanoparticles concentration. The stand-off distance (MQL nozzle-tip to work surface distance) and the nanofluid flow rate were uniform of 30 mm and 60 ml/hr, respectively, for all the experiments and selected based on the literature review and pilot experiments. Each experiment was performed for 10 mm in length. Three components of a cutting force, namely, feed force (*Fx*), radial force (*Fy*), and tangential force (*Fz*), were measured using a strain gauge type cutting force dynamometer. Experimental setup and the components of resultant cutting force are as shown in Figures 2(a) and (b), respectively.

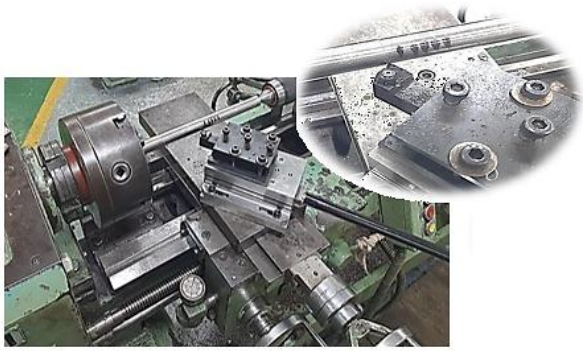

(a)

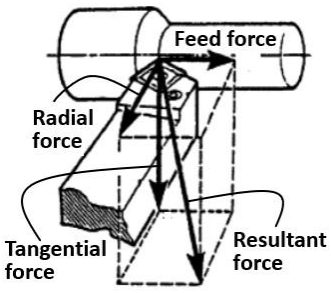

(b)

Fig 2. (a) Experimental setup, (b) Components of cutting force

The resultant force (*Fr*) was obtained using equation (1) or (2).

$$Resultant\ force\ (F_r) = \sqrt{F_x^2 + F_y^2 + F_z^2} \quad (1)$$

Or, resultant force can be expressed as

$$F_r = \left[F_x^2 + F_y^2 + F_z^2\right]^{1/2} \quad (2)$$

Surface roughness was measured using Surfcom 1400G type surface roughness tester. The stylus used for the measurement is a 60^o conical diamond. The material removal rate (*MRR*) is the volume of material removed per minute and obtained using equation (3).

$$MRR\ (mm^3/\text{min}) = 1000\ V\ f\ d \quad (3)$$

where, *V* is the cutting speed of the workpiece (m/min), *f* is feed (mm/rev), and *d* is depth of cut (mm).

3. Results and Discussion

The selection of process parameters for sustainable machining with optimum efficiency is crucial in the case of machining titanium alloys. Numerous efforts have been made to study the machinability of titanium alloys considering the effect of process parameters, tool material, and its geometry, and cooling conditions considering economic, technical, and environmental requirements. In the present study, the machining performance of titanium grade-1 alloy was evaluated in terms of resultant cutting force (*Fr*), machined surface roughness (*Ra*), and material removal rate (*MRR*) through a multi-objective optimization approach.

Turning experiments were performed with CVD-coated TiCN-Al_2O_3 carbide inserts using vegetable oil-based nanofluid under minimum quantity lubrication. The nanofluid was prepared using coconut oil as a base fluid mixed with boron nitride (hBN) nanoparticles. Experiments were performed by varying the cutting speed, feed, depth of cut, and nanoparticles concentration in a base fluid. Three components of a cutting force, namely feed force (*Fx*), radial force (*Fy*), and tangential force (*Fz*), surface roughness, and material removal rate were measured in each experiment. The experimental conditions used in the present study with the results obtained for resultant force (*Fr*), surface roughness (*Ra*), and material removal rate (*MRR*) are as shown in Table 6.

3.1. Mathematical models

In recent years, a significant emphasis has been placed by researchers on the development of predictive models for performance measures during machining. In the present work, empirical equations for *Fr and Ra* are developed for understanding the parametric effect on the machining performance with contour and surface plots.

Table 6
Experimental matrix with performance responses

Expt. no.	*V* (m/min)	*f* (mm/rev)	*d* (mm)	*C* (%)	*Fr* (N)	*Ra* (μm)	*MRR* (mm^3/min)
1	90	0.16	0.5	0.75	396	0.89	7200
2	90	0.16	0.75	1	424	0.97	10800
3	90	0.1	0.1	0.75	307	0.64	900
4	90	0.16	0.1	0.25	301	1.16	1440
5	90	0.2	0.5	1	405	1.3	9000
6	35	0.1	0.1	0.25	311	0.64	350
7	125	0.16	0.75	0.25	393	0.83	15000
8	125	0.2	0.5	0.75	393	1.2	12500
9	90	0.1	0.75	0.25	391	0.4	6750
10	90	0.1	0.5	1	390	0.46	4500
11	90	0.2	0.75	0.75	424	1.42	13500
12	35	0.16	0.5	1	424	1.03	2800
13	35	0.16	0.75	0.75	444	0.95	4200
14	125	0.16	0.5	0.25	371	0.93	10000
15	90	0.16	0.5	0.75	396	1.03	7200
16	90	0.2	0.5	0.25	383	1.31	9000
17	125	0.16	0.1	0.75	308	0.89	2000
18	35	0.16	0.5	0.25	401	1.12	2800
19	90	0.16	0.75	0.25	401	0.89	10800
20	125	0.16	0.5	1	392	0.95	10000
21	125	0.1	0.5	0.25	362	0.5	6250
22	90	0.1	0.5	0.25	369	0.48	4500
23	90	0.16	0.5	0.75	396	0.95	7200
24	90	0.16	0.1	1	318	1.22	1440
25	35	0.16	0.1	0.75	333	0.91	560
26	90	0.2	0.1	0.75	318	1.58	1800
27	35	0.2	0.5	0.75	424	1.22	3500

Regression equations for resultant force (*Fr*) and surface roughness (*Ra*) were developed based on experimental data. The values of the coefficients involved in the equation were calculated by regression method by using the Data-fit software. Empirical models developed to predict response measures during the turning of titanium grade-1 alloy using coconut oil-based hBN nanofluid under MQL are given in Table 7.

Table 7
Empirical models to predict process responses

Process responses	Empirical models	R-squared	Eq. no.
Resultant force (*Fr*) (N)	$= 642.7336V^{-0.0612}f^{0.054}d^{0.1429}C^{0.0402}$	0.875	(4)
Surface roughness (*Ra*) (μm)	$= 13.28896V^{-0.0248}f^{1.4085}d^{-0.0805}C^{-0.006}$	0.905	(5)

R-squared (R^2) is a coefficient of multiple determinations that measures variation proportion in the data points. The equation is significant if the value of R-squared is very close to +1. In the present study, the R-squared values for all the developed models (Table 7) are close to 0.9. Therefore, the empirical equations developed are reliable to predict the resultant force (*Fr*) and surface roughness (*Ra*) during the turning of titanium grade-1 alloy using coconut oil-based hBN nanofluid under MQL (equations (4) and (5)). However, these equations are valid within the range of the parameters selected in the present study for the given combination of tool and workpiece pair.

To have a clear understanding of the effect of a given input parameter on the machining performance, three-dimensional (3-D) surface plots are plotted by varying two of the process parameters at a time considering the central values of the other process parameters as depicted in Table 5. The plots are plotted using developed empirical equations. Figure 3 depicts the 3-D surface plots of resultant cutting force during turning of titanium grade-1 alloy using coconut oil-based hBN nanofluid under MQL plotted using equation (4).

The resultant force can be seen as decreasing with the increase in the cutting speed and increases with the increase in feed and depth of cut, and concentration of hBN nanoparticles in the coconut oil. However, the resultant force can be seen as increasing more prominently with the depth of cut followed by the feed and concentration of nanoparticles. This can be also confirmed from the higher positive exponent value for the depth of cut followed by feed and concentration of nanoparticles from equation (4).

Figure 3(a) depicts the 3-D plot of a resultant force varying with the cutting speed and feed. The lower resultant force observed at higher values of cutting speed could be attributed to softening of the material due to the rise in the cutting temperature during machining. The increase in the resultant force with the increase in the feed and decrease in the cutting speed can be seen. However, resultant force can be seen as varying more prominently with the depth of cut in comparison to cutting speed can be seen from Figure 3(b). The resultant force can be seen as increasing with the increase in the concentration of nanoparticles as shown in Figure 3(c). This could be attributed to a rise in the friction at the chip-tool interface due to the addition of nanoparticles in the cutting fluid. However, a decrease in the resultant force with the increase in cutting speed can be seen as more prominent at lower values of concentration of nanoparticles in the coconut oil.

From Figures 3(d) and (e), the resultant force can be seen as increasing more prominently with the depth of cut and concentration of nanoparticles against the feed. This shows that the selection of depth of cut and concentration of nanoparticles in the base fluid is more significant in obtaining lower resultant force as compared to feed. On the other hand, from Figure 3(f), the depth of cut can be seen as significantly affecting the resultant force as compared to the concentration of nanoparticles in the base fluid.

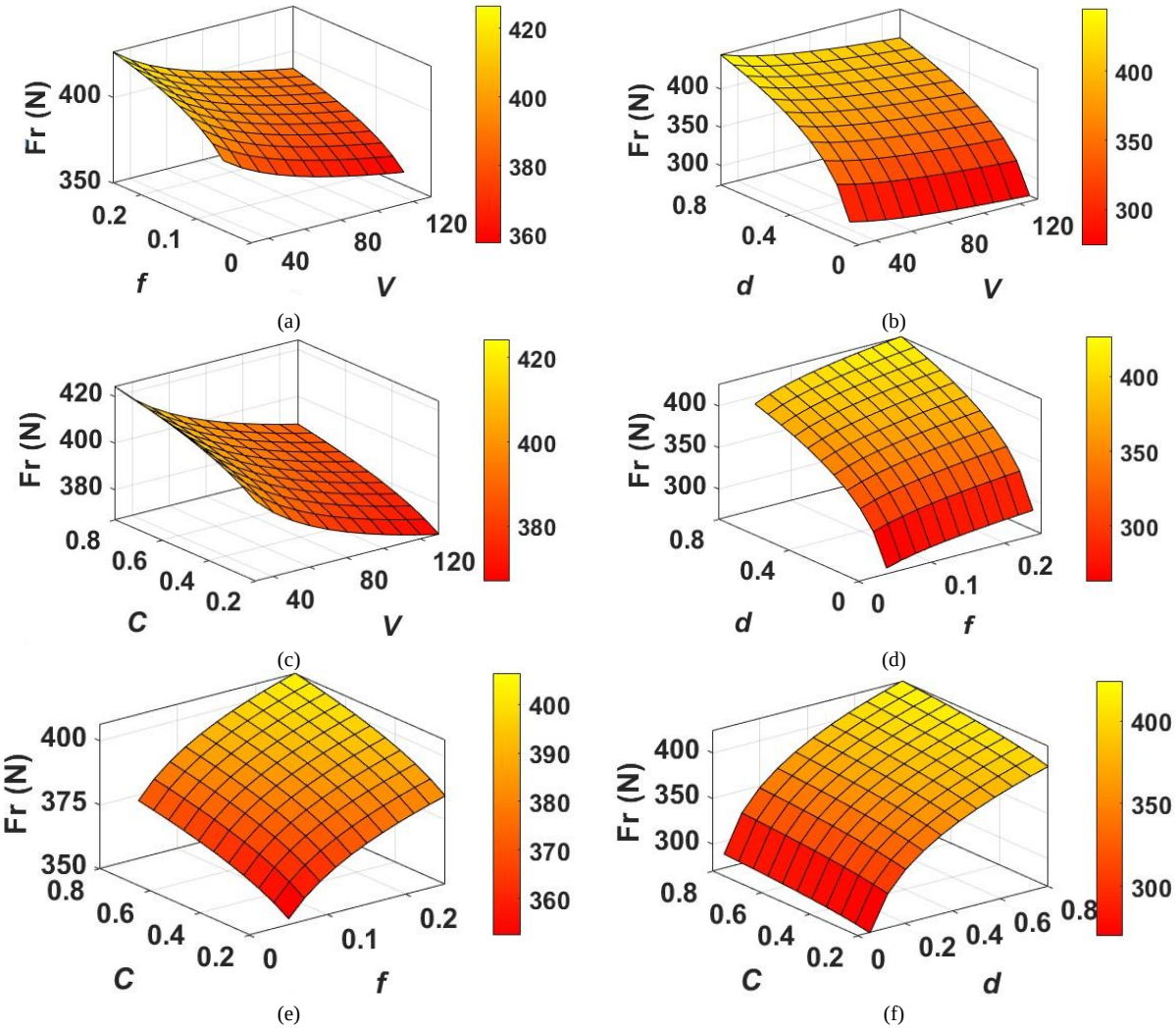

Fig. 3. Resultant cutting force varying with (a) *V* x *f*, (b) *V* x *d*, (c) *V* x *C*, (d) *f* x *d*, (e) *f* x *C*, and (f) *d* x *C*

3-D surface plots showing surface roughness varying with the cutting speed, feed, depth of cut, and concentration of nanoparticles in the base fluid are shown in Figures 4(a) to (f). 3-D surface plots are plotted by varying two of the process parameters at a time considering the central values of the other process parameters as depicted in Table 5. Plots are plotted using equation (5). From Figures 4(a) and (b), the increase in the surface roughness of the machined surface can be seen as more significant with the increase in the feed. The cutting speed can be seen as having a negligible effect on the surface roughness. However, the decrease in surface roughness can be seen with the increase in the depth of cut. The concentration of nanoparticles can be seen as having a negligible effect on the surface roughness in comparison to the cutting speed from Figure 4(c) and feed can be seen as more prominent with respect to depth of cut and concentration of nanoparticles from Figures 4(d) and (e). On the other hand, Figure 4(f) depicts that the depth of cut significantly affects the surface roughness against the concentration of nanoparticles.

The selection of the feed can be seen as more crucial followed by the cutting speed and depth of cut for obtaining the lower surface roughness during turning of titanium grade-1 alloy using coconut oil-based hBN nanofluid under MQL. However, the concentration of nanoparticles has been observed to have a negligible effect on the surface roughness. Lower values of surface roughness and resultant force could be obtained by selecting lower values of feed, depth of cut, and concentration of nanoparticles, and higher values of cutting speed. On the other hand, higher values for the material removal rate could be obtained with higher values of cutting speed, feed, and depth of cut. The objectives, to have minimum surface roughness and resultant force are contradicting with the maximum *MRR* objective. And hence a multi-objective optimization of process parameters needs to be carried out for obtaining the optimum machining performance during the turning of titanium alloy (Grade-1) using vegetable-based nanofluid under MQL. The next section discusses the optimization of process parameters.

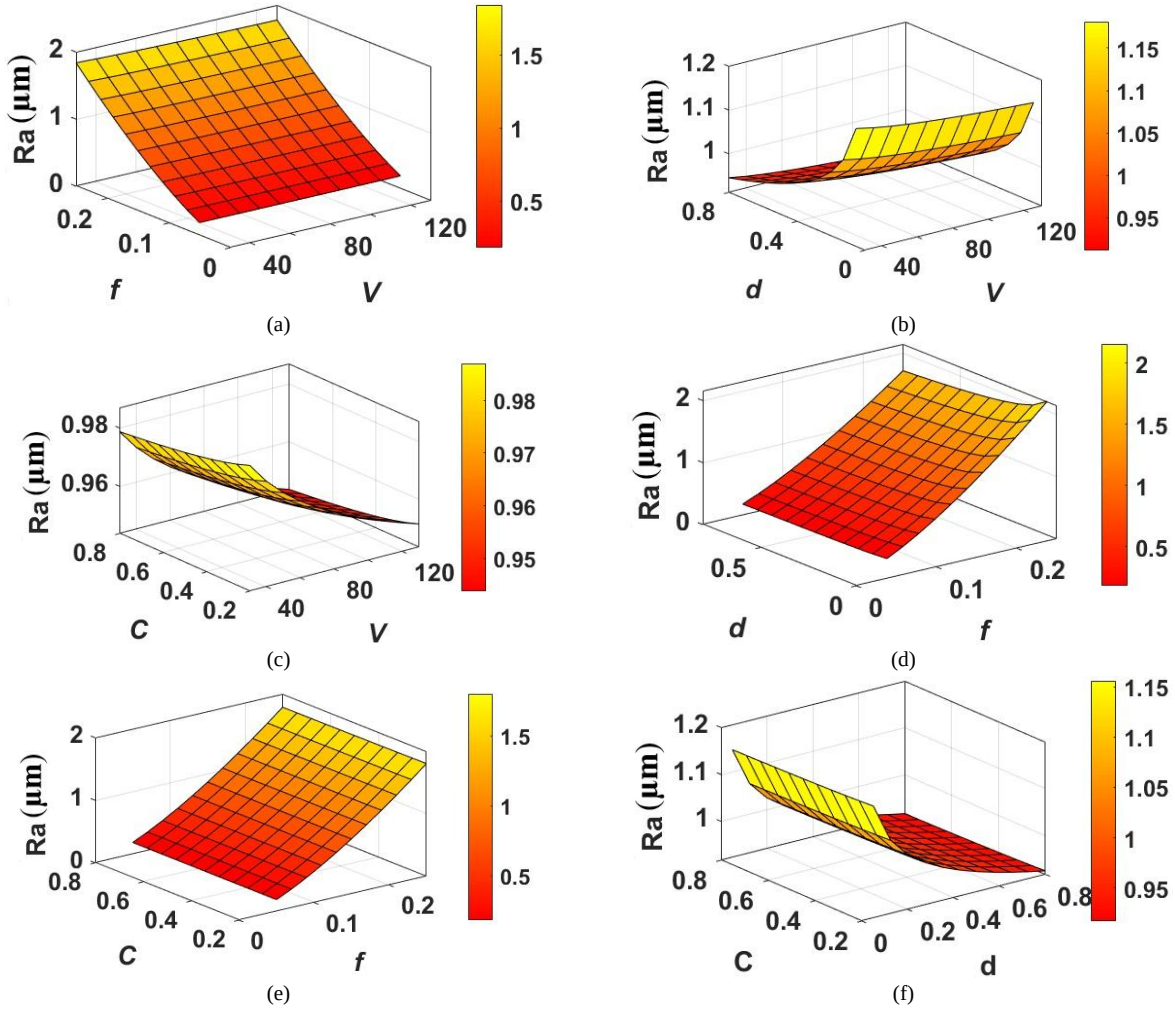

Fig. 4. Surface roughness varying with (a) *V* x *f*, (b) *V* x *d*, (c) *V* x *C*, (d) *f* x *d*, (e) *f* x *C*, and (f) *d* x *C*

4. Multi-Objective Optimization

Several attempts have been made by researchers in the optimization of machining performance. However, very limited studies available in the open literature comprehensively evaluated and optimized the machining performance considering the effect of process parameters during the turning of titanium grade-1 alloy using vegetable-based nanofluid under minimum quantity lubrication (MQL).

Over the years, many classical and non-classical optimization techniques have been developed by researchers for domain engineering applications. In this study, a desirability function approach, a technique for order of preference by similarity to ideal solution (TOPSIS), Grey Relational Analysis (GRA), and non-dominated sorting genetic algorithm (NSGA-II) are used for simultaneous optimization of process responses, namely, minimum resultant force, minimum surface roughness, and maximum material removal rate.

4.1. The Desirability Function Approach (DFA)

With this approach, each response variable is transformed into desirability function (*Di*) using equation (6) and optimization of several response variables (*Ri*) are converted into the optimization of single desirability function, 'D_M' using equation (7).

$$Di = \left\{ \begin{matrix} 0,1 \\ \frac{R_i - R_{min}}{R_{max} - R_{min}} \\ 1,0 \end{matrix} \right\}_i \begin{matrix} R_i \le R_{min} \\ , R_{min} < R_i < R_{max} \\ R_i \ge R_{max} \end{matrix} \quad (6)$$

$$D_M = (D_1 * D_2 * D_3 * - - - * D_n)^{1/n} \quad (7)$$

Each response '*Ri*' is transformed into its respective '*Di*' by using a one-sided transformation (Chinchanikar and Choudhury, 2013). In the present study, the goal was to find the optimum values of cutting speed, feed, depth of cut, and concentration of nanoparticles in the base fluid for minimum resultant force, minimum surface roughness, and maximum MRR. Process variables and the range of process responses are given in Table 8.

Table 8
Process variables and the range of process responses

Process parameters and responses	Goal	Min. limit	Max. limit
Cutting speed (*v*) (m/min)	Is in range	30	125
Feed (*f*) (mm/rev)	Is in range	0.1	0.2
Depth of cut (*d*) (mm)	Is in range	0.1	0.75
Concentration (C) (%)	Is in range	0.25	1
Resultant force (*Fr*)	Minimize	301	444
Surface roughness (*Ra*)	Minimize	0.4	1.58
Material removal rate (*MRR*)	Maximize	350	15000

Minimum and maximum limits of the resultant force, surface roughness, and *MRR* are referred to from experimental observations as depicted in Table 6. One-sided transformation for resultant force (equation 8), surface roughness (equation 9), and material removal rate (equation 10) can be expressed by substituting the minimum and maximum limits of the corresponding responses as shown in Table 9.

For the optimization study, different combinations of process parameters were selected in the range depicted in Table 8. The cutting speed was varied in steps of 4.5 in the range of 35 to 125 m/min, feed varied in steps of 0.005 in the range of 0.1 to 0.2 mm/rev, depth of cut in steps of 0.0325 in the range of 0.1 to 0.75 mm, and nanoparticles concentration in steps of 0.375 in the range of 0.25 to 1 %.

For each level of independent parameters, 'D_{Fr}' (Desirability for resultant force), 'D_{Ra}' (Desirability for surface roughness), and 'D_{MRR}' (desirability for material removal rate) were calculated using equations (8)-(10) as shown in Table 9. Then, a single desirability function 'D_M' (Desirability for minimum *Fr*, minimum *Ra*, and maximum *MRR*) was calculated by substituting the values of 'D_{Fr}', 'D_{Ra}', and 'D_{MRR}' in equation (7). The solution having the highest desirability level ('D_M') was selected as an optimum solution for turning titanium grade-1 alloy using coconut oil-based hBN nanofluid under MQL. The family of optimum solutions obtained is shown in Table 10.

The desirability function approach (DFA) suggests a family of optimum solutions for minimum resultant force, minimum surface roughness, and maximum MRR as depicted in Table 10. DFA optimization technique suggests that the cutting speed in the range of 120-125 m/min, feed of 0.1-0.12 mm/rev, depth of cut of 0.71-0.75 mm, and concentration of hBN nanoparticles in the range of 0.25-0.325% in coconut oil are the optimum parameters. The optimization study reveals that minimum resultant force in the range of 382-388 N, the minimum surface roughness of 0.47-0.61 μm, and maximum *MRR* in the range of 8875-11250 mm^3/min could be obtained using process parameters as shown in Table 10.

Table 9.
One sided transformation for process responses for *Fr*, *Ra*, and *MRR*

Sr. no.	Process responses	Desirability for	Eq. no.
1	Resultant cutting force (*Fr*)	$D_{Fr} = \begin{Bmatrix} 0, & Fr \geq 444 \\ \frac{Fr_{max} - Fr_i}{Fr_{max} - Fr_{min}} \\ 1, & Fr \leq 301 \end{Bmatrix}, Fr_{min} < Fr_i < Fr_{max}$	(Eq. 8)
2	Surface roughness (*Ra*)	$D_{Ra} = \begin{Bmatrix} 0, & Ra \geq 1.58 \\ \frac{Ra_{max} - Ra_i}{Ra_{max} - Ra_{min}} \\ 1, & Ra \leq 0.4 \end{Bmatrix}, Ra_{min} < Ra_i < Ra_{max}$	(Eq. 9)
3	Material removal rate (*MRR*)	$D_{MRR} = \begin{Bmatrix} 0, & MRR \leq 350 \\ \frac{MRR_i - MRR_{min}}{MRR_{max} - MRR_{min}} \\ 1, & MRR \geq 15000 \end{Bmatrix}, MRR_{min} < MRR_i < MRR_{max}$	(Eq. 10)

Table 10.
Optimum process parameters using desirability function approach (DFA)

Sr. No.	Speed (m/min)	Feed (mm/rev)	Depth of cut (mm)	% Concentration	F_R (N)	*Ra* (μm)	*MRR* (mm^3/min)
1	125	0.1	0.75	0.325	388	0.47	9375
2	125	0.1	0.75	0.25	383	0.47	9375
3	120.5	0.1	0.75	0.25	384	0.48	9037.5
4	125	0.1	0.75	0.2875	386	0.47	9375
5	125	0.11	0.71	0.25	382	0.55	9762.5
6	125	0.12	0.75	0.25	387	0.61	11250

4.2. Technique for Order Preference by Similarity to Ideal Solution (TOPSIS)

This section discusses the simultaneous optimization of process responses, namely, minimum resultant force, minimum surface roughness, and maximum material removal rate considering the effect of process parameters using a Technique for Order of Preference by Similarity to Ideal Solution (TOPSIS). This technique was developed by Hwang and Yoon in the year 1995. This method works on the concept that the selected process parameter should be at the shortest distance from the best solution (Positive ideal solution) and the longest distance from the worst solution (negative idle solution) (Rao, 2011).

In the present work, the TOPSIS method has been applied to convert the multi-objective responses to an equivalent single objective response. The TOPSIS methodology, i.e., the steps followed to convert the multi-response problems into the single response problem for obtaining the optimized parameters for minimum Fr, minimum Ra, and maximum MRR is shown in Figure 5.

The process response matrix (decision matrix) is normalized by using equation (11). The weight for each response is calculated. The weighted normalized process response matrix is then calculated by multiplying the normalized process response matrix (decision matrix) by its associated weights using equation (12). Then positive ideal solution (S+) and the negative ideal solution (S-) are determined using equations (13) and (14). Further, the separation of each alternative from positive ideal solution (S+) and negative ideal solution (S-) is calculated using equations (15) and (16). Finally, the closeness coefficient of each alternative (CC*i*) is calculated using equation (17). Normalized, weighted normalized values, positive ideal, negative ideal solutions, separation measures, closeness coefficient values, and rank are depicted in Table 11.

The TOPSIS results show that the rank 1 solution is the optimum solution for experiment number 7 as shown in Table 11. The process parameters for optimum results listed at experiment number 7 can be referred from Table 6. It has been observed that the cutting speed of 125 m/min, feed of 0.16 mm/rev, depth of cut of 0.75 mm, and concentration of hBN nanoparticles of 0.25% in coconut oil are the optimum parameters. Setting these parameters, the minimum resultant force of 393 N, the minimum surface roughness of 0.83 μm, and the maximum MRR of 15000 mm3/min can be obtained (Table 6). However, validatory experiments are required to confirm the accuracy of the results. This has been observed that using TOPSIS one cannot have the freedom to select an optimum solution from a family of optimal solutions as obtained with the DFA technique.

Table 11
TOPSIS process response matrix with optimum solutions ranking

Expt. no.	Normalized results			Normalized weighted matrix			Separation measures		Closeness coefficient	Rank
	Fr	*Ra*	*MRR*	*Fr*	*Ra*	*MRR*	S^+	S^-	*CCi*	
1	0.2008	0.1709	0.1861	0.0669	0.0570	0.0620	0.075857	0.07415	0.494307	10
2	0.2153	0.1862	0.2791	0.0718	0.0621	0.0930	0.055446	0.098169	0.639059	4
3	0.1556	0.1229	0.0233	0.0519	0.0410	0.0078	0.12242	0.064676	0.345682	17
4	0.1527	0.2227	0.0372	0.0509	0.0742	0.0124	0.126519	0.0374	0.228163	25
5	0.2056	0.2496	0.2326	0.0685	0.0832	0.0775	0.079366	0.076915	0.49216	12
6	0.1577	0.1229	0.0090	0.0526	0.0410	0.0030	0.127129	0.064248	0.335715	19
7	0.1996	0.1593	0.3876	0.0665	0.0531	0.1292	0.03164	0.135281	0.810452	1
8	0.1992	0.2304	0.3230	0.0664	0.0768	0.1077	0.057661	0.107797	0.651507	3
9	0.1985	0.0768	0.1744	0.0662	0.0256	0.0581	0.072683	0.093921	0.563738	8
10	0.1981	0.0883	0.1163	0.0660	0.0294	0.0388	0.091778	0.080607	0.4676	14
11	0.2154	0.2726	0.3488	0.0718	0.0909	0.1163	0.06974	0.113778	0.619984	6
12	0.2153	0.1977	0.0724	0.0718	0.0659	0.0241	0.114467	0.041177	0.26456	22
13	0.2255	0.1824	0.1085	0.0752	0.0608	0.0362	0.102375	0.0522	0.337702	18
14	0.1883	0.1785	0.2584	0.0628	0.0595	0.0861	0.05609	0.093766	0.62571	5
15	0.2008	0.1977	0.1861	0.0669	0.0659	0.0620	0.079977	0.06919	0.463843	16
16	0.1945	0.2515	0.2326	0.0648	0.0838	0.0775	0.079093	0.077177	0.49387	11
17	0.1564	0.1709	0.0517	0.0521	0.0570	0.0172	0.116289	0.05178	0.30809	20
18	0.2036	0.2150	0.0724	0.0679	0.0717	0.0241	0.115987	0.036945	0.241578	23
19	0.2036	0.1709	0.2791	0.0679	0.0570	0.0930	0.050792	0.100521	0.664324	2
20	0.1991	0.1824	0.2584	0.0664	0.0608	0.0861	0.057731	0.092796	0.616474	7
21	0.1836	0.0960	0.1615	0.0612	0.0320	0.0538	0.076337	0.08691	0.532382	9
22	0.1873	0.0921	0.1163	0.0624	0.0307	0.0388	0.091319	0.079962	0.466846	15
23	0.2008	0.1824	0.1861	0.0669	0.0608	0.0620	0.077523	0.07193	0.481286	13
24	0.1615	0.2342	0.0372	0.0538	0.0781	0.0124	0.128077	0.032774	0.203754	26
25	0.1691	0.1747	0.0145	0.0564	0.0582	0.0048	0.128704	0.046846	0.26685	21
26	0.1615	0.3033	0.0465	0.0538	0.1011	0.0155	0.136518	0.024702	0.153219	27
27	0.2154	0.2342	0.0904	0.0718	0.0781	0.0301	0.114024	0.035752	0.238702	24

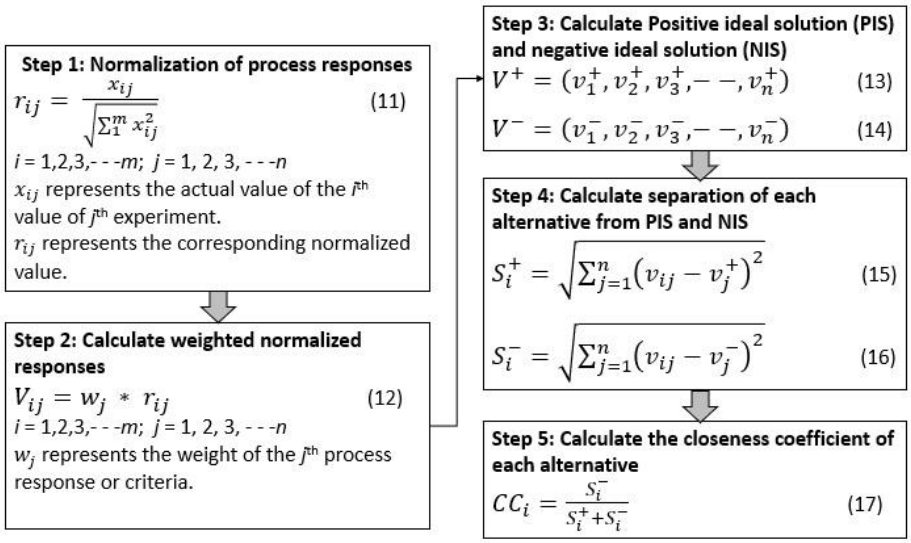

Fig. 5. TOPSIS methodology

4.3. Grey Relational Analysis (GRA)

Grey Relational Analysis (GRA) was developed for the optimization of multi-performance characteristics (Lin and Tarng, 1998). The analysis is based on linear normalization of the data in the range between zero and one, which is also called the Grey Relational generating.

A group of researchers has used GRA for solving the complicated interrelationships and to analyze the multi-objective process responses. In this technique, the Grey Relational grade (GRG) is obtained as an indicator for the evaluation of multi-objective process responses. In GRA, the complex multiple response optimization problems can be simplified into the optimization of a single response. The GRG converts the multi-objective optimization problem (multiple responses) into a single objective optimization problem (single response). The steps to be followed to obtain the GRG are shown in Figure 6.

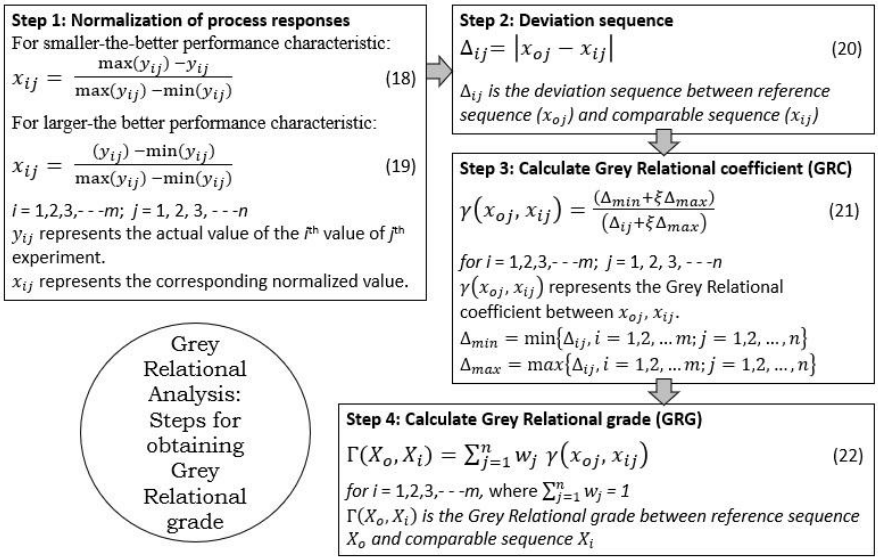

Fig 6. Grey Relational analysis methodology

In GRA, in step one, all process responses (the actual data) are transformed to a comparability sequence. This transformation is called Grey Relational generating. In this step, data are normalized and transformed to values in 0-1 interval to avoid the effect of adopting different units and to reduce the variability. After that, in the further steps, the Grey Relational coefficient (GRC) is evaluated on normalized data to show the relationship between the predicted and actual data.

In the first step, process responses are transformed from the original sequence to a comparable sequence. Numerical data are normalized between zero and one. In this study, the normalized value of the original sequence for resultant cutting force and surface roughness are smaller-the-better performance characteristics and can be expressed as equation (18). The normalized value of the original sequence for material removal rate is a larger-the-better performance characteristic and can be expressed as equation (19). The performance of experiment i is considered as the best for the response j if the value xij is equal to 1 or nearer to 1 than the value for any other experiment. The reference sequence X0 is defined as (x01, x02, …, x0j, …, x0n) = (1, 1, …, 1, …, 1), where x0j is the reference value for jth response and it aims to find the experiment whose comparability sequence is the closest to the reference sequence (Jozić et al., 2015). Considering this sequence, a reference (ideal target) sequence is defined, and deviation sequences are obtained using equation (20).

Then, the GRC is calculated using equation (21) to determine how close the reference sequence (x0j) is to all comparability sequences (xij). The term in equation (21) ξ is a distinguishing coefficient in [0, 1] and its value is usually 0.5 in literature.

The distinguishing coefficient (ξ) is the index for distinguishability. The smaller the ξ, the higher its distinguishability. In the present study, the value for ξ is considered as 0.5. The larger the grey relational coefficient, the closer is xij and x0j. Finally, GRG between the reference sequence and comparability sequences is a weighted sum of Grey Relational coefficients (GRCs) and calculated using equation (22). The weight of response j is wj and usually depends on decision makers' judgment. In the present study, equal weights are considered for all three responses.

If an experiment gets the highest grey relational grade with the reference sequence, it means that the comparability sequence is most like the reference sequence and that experiment would be the best choice. The highest grey relational grade among the process responses is selected as the best option. Table 12 shows the GRA response matrix with GRCs and GRG for each experiment. The highest Grey Relational grade is the order of 1.

Table 12.
Grey relational analysis (GRA) response matrix with Grey grade and rank

Expt. no.	Normalized results			Deviation sequences			Grey relational coefficients			Grey grade	Grey Rank
	Fr	Ra	MRR	Fr	Ra	MRR	Fr	Ra	MRR		
1	0.3385	0.5847	0.4676	0.6615	0.4153	0.5324	0.4305	0.5463	0.4843	0.4870	19
2	0.1400	0.5169	0.7133	0.8600	0.4831	0.2867	0.3676	0.5086	0.6356	0.5039	17
3	0.9602	0.7966	0.0375	0.0398	0.2034	0.9625	0.9263	0.7108	0.3419	0.6597	2
4	1.0000	0.3559	0.0744	0.0000	0.6441	0.9256	1.0000	0.4370	0.3507	0.5959	8
5	0.2726	0.2373	0.5904	0.7274	0.7627	0.4096	0.4074	0.3960	0.5497	0.4510	23
6	0.9308	0.7966	0.0000	0.0692	0.2034	1.0000	0.8785	0.7108	0.3333	0.6409	3
7	0.3561	0.6356	1.0000	0.6439	0.3644	0.0000	0.4371	0.5784	1.0000	0.6718	**1**
8	0.3607	0.3220	0.8294	0.6393	0.6780	0.1706	0.4389	0.4245	0.7455	0.5363	11
9	0.3705	1.0000	0.4369	0.6295	0.0000	0.5631	0.4427	1.0000	0.4703	0.6377	4
10	0.3764	0.9492	0.2833	0.6236	0.0508	0.7167	0.4450	0.9077	0.4109	0.5879	9
11	0.1386	0.1356	0.8976	0.8614	0.8644	0.1024	0.3673	0.3665	0.8300	0.5212	14
12	0.1403	0.4661	0.1672	0.8597	0.5339	0.8328	0.3677	0.4836	0.3752	0.4088	26
13	0.0000	0.5339	0.2628	1.0000	0.4661	0.7372	0.3333	0.5175	0.4041	0.4183	24
14	0.5103	0.5508	0.6587	0.4897	0.4492	0.3413	0.5052	0.5268	0.5943	0.5421	10
15	0.3385	0.4661	0.4676	0.6615	0.5339	0.5324	0.4305	0.4836	0.4843	0.4661	22
16	0.4258	0.2288	0.5904	0.5742	0.7712	0.4096	0.4654	0.3933	0.5497	0.4695	21
17	0.9489	0.5847	0.1126	0.0511	0.4153	0.8874	0.9073	0.5463	0.3604	0.6047	6
18	0.3006	0.3898	0.1672	0.6994	0.6102	0.8328	0.4169	0.4504	0.3752	0.4141	25
19	0.3004	0.5847	0.7133	0.6996	0.4153	0.2867	0.4168	0.5463	0.6356	0.5329	12
20	0.3620	0.5339	0.6587	0.6380	0.4661	0.3413	0.4394	0.5175	0.5943	0.5171	16
21	0.5752	0.9153	0.4027	0.4248	0.0847	0.5973	0.5407	0.8551	0.4557	0.6171	5
22	0.5240	0.9322	0.2833	0.4760	0.0678	0.7167	0.5123	0.8806	0.4109	0.6013	7
23	0.3385	0.5339	0.4676	0.6615	0.4661	0.5324	0.4305	0.5175	0.4843	0.4774	20
24	0.8797	0.3051	0.0744	0.1203	0.6949	0.9256	0.8061	0.4184	0.3507	0.5251	13
25	0.7747	0.5678	0.0143	0.2253	0.4322	0.9857	0.6894	0.5364	0.3365	0.5208	15
26	0.8787	0.0000	0.0990	0.1213	1.0000	0.9010	0.8047	0.3333	0.3569	0.4983	18
27	0.1389	0.3051	0.2150	0.8611	0.6949	0.7850	0.3673	0.4184	0.3891	0.3916	27

The highest Grey Relational grade of the order of 1 can be seen for experiment number 7. This shows the nearest optimum cutting condition with cutting speed of 125 m/min, feed of 0.16 mm/rev, depth of cut of 0.75 mm, and concentration of nanoparticles of 0.25%. With these parameters, the minimum resultant force of 393 N, the

minimum surface roughness of 0.83 μm, and the maximum *MRR* of 15000 mm^3/min can be obtained (Table 6). However, validatory experiments are required to confirm the accuracy of the results. The optimization solutions obtained with TOPSIS and GRA are the same. However, with TOPSIS and GRA one cannot have the freedom to select an optimum solution from a family of optimal solutions as obtained with the DFA technique.

4.4 Non-dominated Sorting Genetic Algorithm II (NSGA-II)

Non-dominated sorting genetic algorithm-II (NSGA-II), a modified version of NSGA, is a popular non-domination-based genetic algorithm for multi-objective optimization as being having a better sorting algorithm, incorporating elitism, and no need to defining sharing parameter a priori. NSGA lacks an elitist approach, has high computational complexity, and needs for function sharing. The complexity of the NSGA approach for sorting and function sharing is of the order of O(MN3), where M be the number of objectives and N is the population size. However, for the NSGA-II approach, the complexity for non-dominance sorting is O(MN2). In NSGA-II the chromosome with the least rank and highest Euclidean distance is considered as the best solution (Deb et al., 2002).

In the single-objective optimization problem, the superiority of a solution over other solutions can be easily determined by comparing their objective function values. However, in a multi-objective optimization problem, the goodness of a solution is determined by dominance. The non-dominated solution set is a set of all the solutions that are not dominated by any member of the solution set. The non-dominated set of the entire feasible decision space is called the Pareto-optimal set. The boundary defined by the set of all points mapped from the Pareto optimal set is called the Pareto optimal front.

A group of researchers attempted modeling and multi-objective optimization using different metaheuristic algorithms, including NSGA-II for the transportation-location-routing problem (Maadanpour Safari, 2021), warranty model with consideration of customer and manufacturer objectives (Asadi et al., 2019), and airport gate scheduling with controllable processing times (Khakzar Bafruei, 2018). The NSGA-II algorithm for obtaining a family of multi-objective optimum solutions is shown in Figure 7.

Initially, the population needs to be initialized and then required to sort based on non-domination into each front. Every individual in each front is assigned a rank (fitness value). A crowding distance, which is a measure of how close an individual is to its neighbors, is obtained for every individual. Better diversity in the population can be obtained by having individuals with large crowding distances. Based on the rank and crowding distance parents are selected from the population using a binary tournament selection. The selected population generates offsprings from crossover and mutation operators. Using non-domination again the population with the current population and current offsprings is sorted and only the best N (Population size) individuals are selected based on rank and the crowding distance.

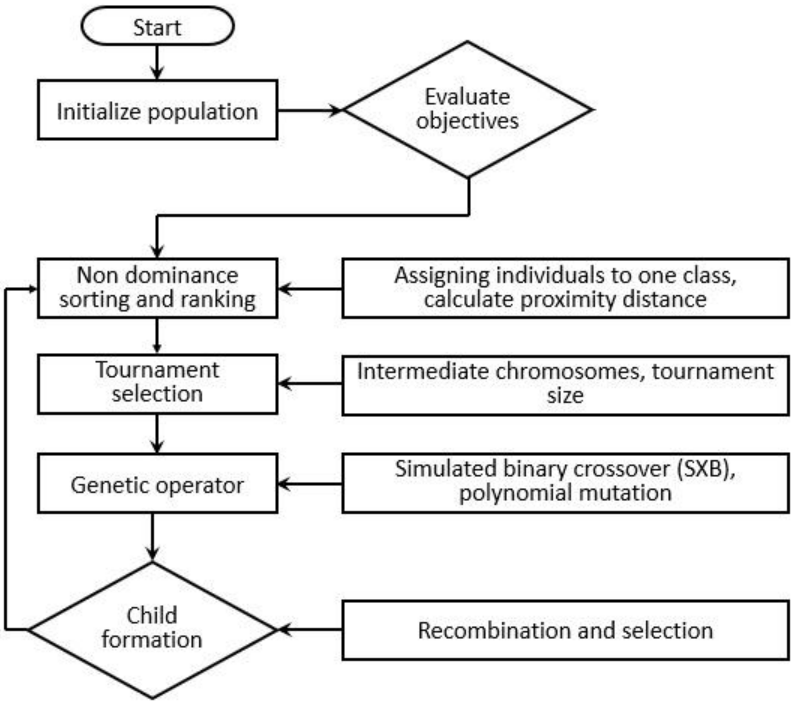

Fig 7. NSGA II algorithm for multi-objective optimization

In the present study of the multi-objective optimization, initially, the population is initialized based on the range of the process parameters. Then initialized population is sorted based on non-domination using the fast sort algorithm. Once the non-dominated sort is completed, all the individuals in the population are assigned a crowding distance value. Once the individuals are sorted based on non-domination and with crowding distance assigned, the selection is carried out using a crowded comparison operator. The individuals are selected by using a binary tournament selection with a crowded comparison operator. Real-coded GA's which use simulated binary crossover (SBX) operator were applied for crossover and used polynomial mutation. Then the offspring population is combined with the current generation population and selection is performed to set the individuals of the next generation. Elitism is ensured as all the previous and current best individuals are added to the population and then the population is sorted based on non-domination. The parameters used in the present study for NSGA-II for the multi-objective problem are depicted in Table 13.

Table 13.
NSGA-II parameters setting for multi-objective optimization

Parameters	Values
Population size	1000
Generation	100
Crossover probability	0.8
Crossover constant	0.5
Mutation probability	0.5
Mutation constant	20

At each generation, the best chromosomes are selected and replaced based on their rank and crowding distance. Population replaced at each generation. Each front is filled in ascending order until the addition of population size is reached. The last front is included in the population based on the individuals with the least crowding distance. Individuals in the first front are given a rank of 1, the second front individuals are assigned rank 2, and so on. After assigning the rank the crowding in each front is calculated. Figure 8 shows the Pareto plots between the objective functions for a complete population of 1000 chromosomes.

Figure 8(a) depicts the Pareto plot for resultant force versus the material removal rate. The Pareto plots represent the potential trade-offs between multi-objective functions. They can be aligned to offer the best fit and worst fit scenarios among the objective functions. The higher *MRR* of about 10000 mm^3/min could be optimally achieved with a little higher resultant force in the range of 370-400 N can be seen. Similarly, Figure 8(b) depicts that the surface roughness of about 0.47-0.5 µm could be optimally achieved with a higher *MRR* of about 10000 mm^3/min. And a lower surface roughness in the range of 0.47-0.55 µm could be optimally obtained with resultant force in the range of 370-410 N (Figure 8(c)) during the turning of titanium grade-1 alloy using coconut oil-based hBN nanofluid. The material removal rate versus surface roughness shows an opposing behavior while *MRR* versus resultant force (*Fr*) shows allied behavior. Surface roughness versus resultant force can be seen as having opposing behavior Pareto plots.

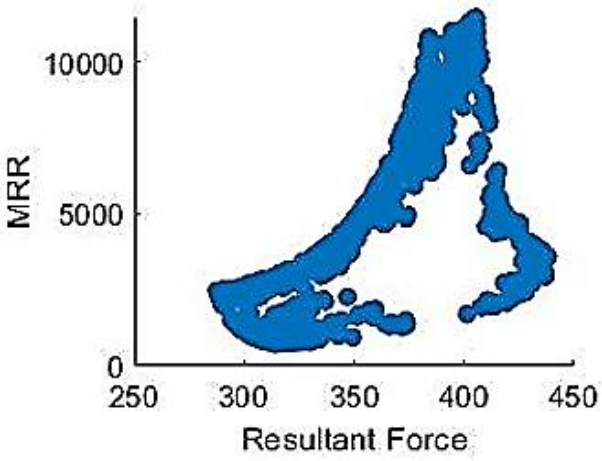

(a)

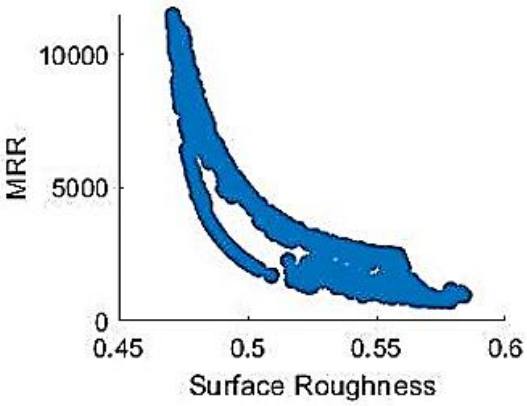

(b)

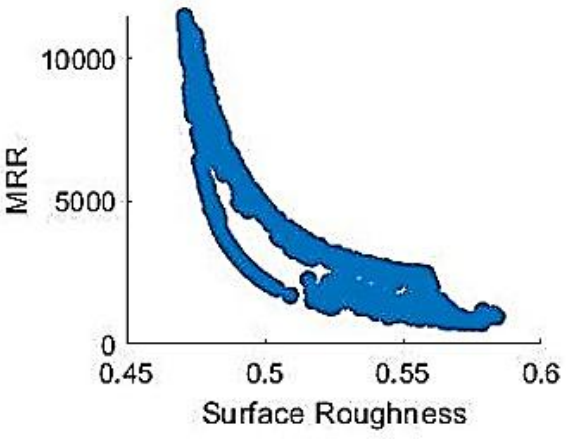

(c)

Fig. 8. Pareto plots for complete population, (a) *Fr* Vs *MRR*, (b) *Ra* Vs *MRR*, and (c) *Fr* Vs *Ra*

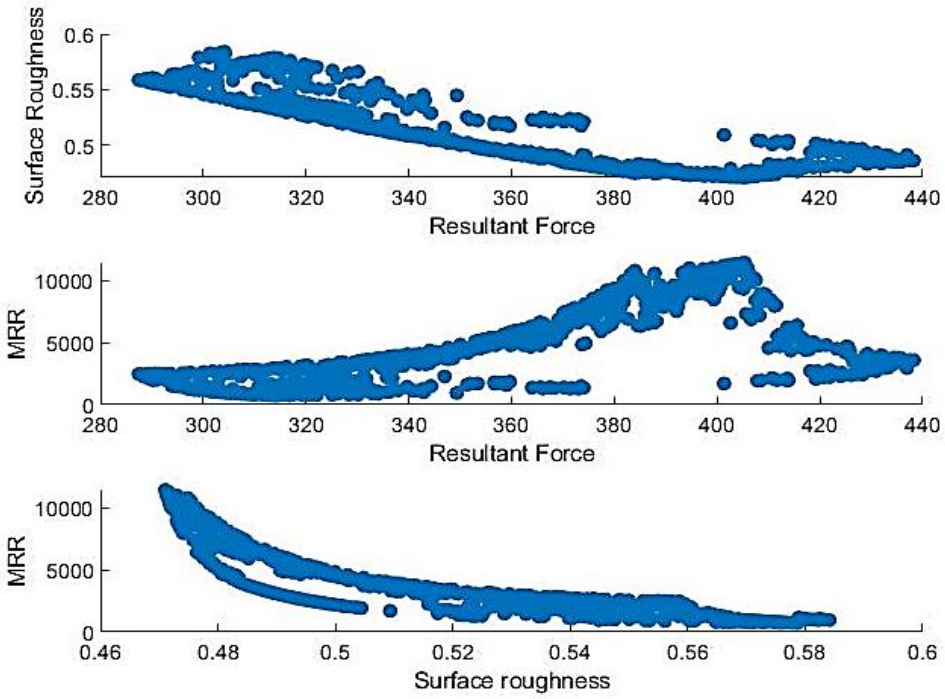

Fig. 9. Pareto plots between the objective functions for child chorosome

Figure 9 depicts Pareto plots between the objective functions for the child chromosome. The Pareto plot shows optimal chromosomes replacing intermediate chromosomes at the final generation and their correlations with each objective function. The demography of each curve is the outcome of the selection and genetic operation at the final generation. These are discrete scatter plots of objective functions selected based on ranks assigned to non-sorted dominant fronts. Surface roughness versus resultant force plot shows that surface roughness is a negative differential to resultant force. *MR*R versus resultant force plot depicts a mix of positive and negative differential. However, *MRR* versus surface roughness shows a negative differential. The tendency of chromosomes reflects that they are biased towards maximizing respective objective functions at extreme ends. The direction of declination shows that surface roughness improves with a gradual decrease in force.

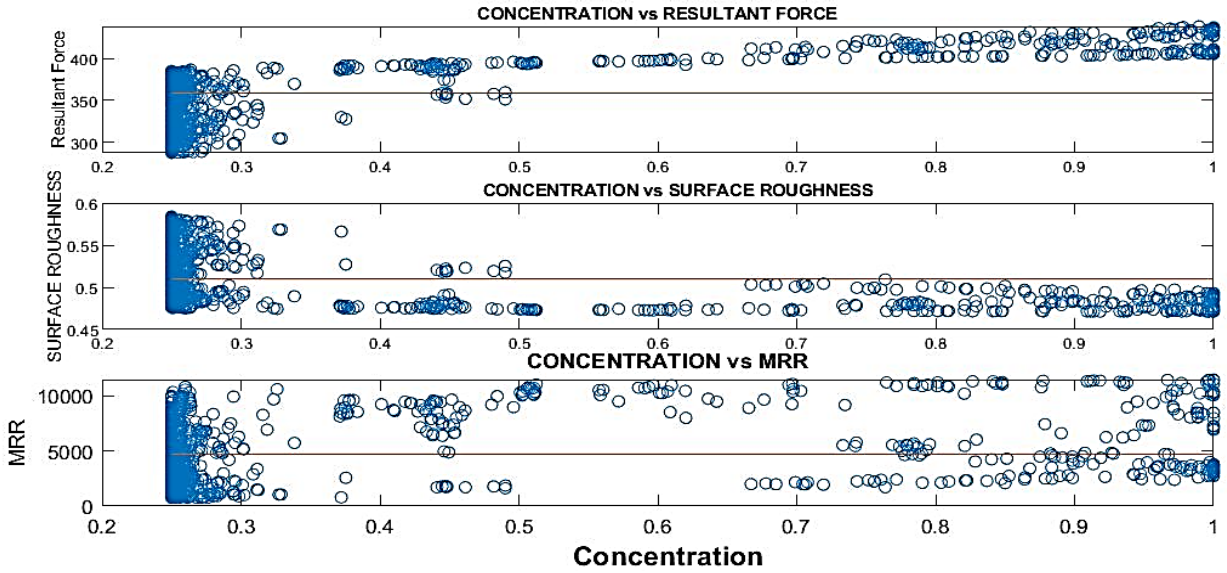

Fig. 10. Optimal solutions corresponding to concentration of nanoparticles

Figures 10 and 11 show that the influence of objective functions with decision variables obtained from optimal chromosomes. On an overview, most of the optimized solutions correspond to minimum concentration for all the objective functions as shown in Figure 10. However, some solutions can be seen as inclined towards a higher concentration of nanoparticles. The mean line in the graph shows that how the solutions maneuvers between global maxima and minima.

Surface roughness solutions are grouped around minimum concentration ranging between 0.25-0.35 µm with few solutions ranging under the mean line. Optimal resultant force solutions are grouped around the minimum concentration of nanoparticles with a few solution sets showing an increase in the resultant force with the increase in the concentration of nanoparticles. Maximum *MRR* corresponds at both the extremes of concentrations with a maximum group of solutions clustered at minimum concentration. Few solutions cover the overall search area oscillating around the mean line of *MRR*. The mean line here acts as a region classifier to determine between best-fit solutions' most optimal and least optimal solutions.

Figure 11 shows the objective functions respond to a depth of cut. A gradual growth in the resultant force with the depth of cut and optimal solutions clustering at both extremes can be seen. A majority of surface roughness optimal solutions can be seen below the mean line of surface roughness and for higher depth of cut. Most optimal solutions for *MRR* can be seen clustered at higher depth of cut.

The objectives in the best fit chromosomes show that the solutions are optimized for minimum feed, maximum cutting speed, maximum depth of cut, and at minimum concentration of nanoparticles in the base fluid. The family of optimized process parameters revealed from NSGA-II is shown in Table 14.

NSGA-II optimization technique suggests a family of optimum solutions for minimum resultant force, minimum surface roughness, and maximum material removal rate. The cutting speed in the range of 119-125 m/min, feed of 0.1 mm/rev, depth of cut of 0.55-0.75 mm, and concentration of hBN nanoparticles in the range of 0.25-0.29% in coconut oil are the optimum parameters. The optimization study reveals that minimum resultant force in the range of 369-392 N, the minimum surface roughness of 0.47-0.49 µm, and maximum *MRR* in the range of 6545-9375 mm^3/min could be obtained.

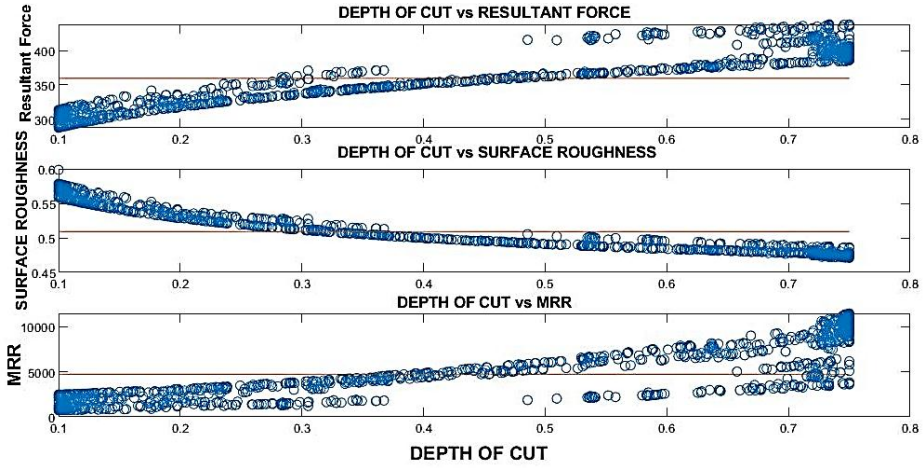

Fig. 11. Optimal solutions corresponding to depth of cut

Table 14
Optimum process parameters using NSGA-II

Sr. No.	Speed (m/min)	Feed (mm/rev)	Depth of cut (mm)	% Concentration	F_R (N)	*Ra* (µm)	*MRR* (mm^3/min)
1	125	0.1	0.75	0.29	392	0.47	9375
2	121	0.1	0.73	029	386	0.48	8833
3	123	0.1	0.56	0.26	369	0.49	6888
4	121	0.1	0.57	0.25	370	0.49	6897
5	119	0.1	0.55	0.25	369	0.49	6545
6	123	0.1	0.56	0.26	369	0.49	6888

Table 15
Optimized parameters with different techniques

Optimization techniques	Optimized process parameters				Optimized process performance		
	Cutting speed (*V*) (m/min)	Feed (*f*) (mm/rev)	Depth of cut (*d*) (mm)	% Concentration	Resultant force (*Fr*) (N)	Surface roughness (*Ra*) (µm)	MRR (mm^3/min)
DFA	125	0.1	0.75	0.325	388	0.47	9375
TOPSIS	125	0.16	0.75	0.25	393	0.83	15000
GRA	125	0.16	0.75	0.25	393	0.83	15000
NSGA-II	125	0.1	0.75	0.29	392	0.47	9375

4.4. Confirmatory experiments

The accuracy of the predicted optimized results of the resultant force, surface roughness, and material removal rate is assessed by experimenting with optimum process parameters. The optimum process parameters revealed from different optimization techniques are shown in Table 15. Almost all the optimization techniques suggested a higher cutting speed of 125 m/min, lower feed rate of 0.1 mm/rev, higher depth of cut of 0.75 mm, and nanoparticles concentration of 0.3% as optimum parameters for lower surface roughness, lower resultant force, and maximum material removal rate.

The confirmatory experiment is performed at the above-mentioned optimum process parameters to check the accuracy of the predicted results. The confirmatory experiment is performed at a cutting speed of 125 m/min, feed of 0.1 mm/rev, depth of cut of 0.75 mm, and using a concentration of nanoparticles of 0.3 %, and the same is repeated thrice as depicted in Table 16. It has been observed that the average resultant force and surface roughness of 387 N and 0.47 µm, respectively, and maximum *MRR* of 9375 mm3/min could be obtained using the cutting speed, feed, depth of cut, and hBN nanoparticles concentration of 125 m/min, 0.1 mm/rev, 0.75 mm, and 0.3%, respectively during turning of titanium grade-1 alloy using coconut oil-based hBN nanofluid under MQL. However, little compromising on the surface roughness to a higher value of 0.83 µm with resultant force of 392 N, the higher MRR of 15000 mm3/min could be obtained using cutting speed of 125 m/min, feed of 0.16 mm/rev, depth of cut of 0.75 mm, and nanoparticle concentration of 0.25%.

This study finds that non-dominated sorting genetic algorithm II (NSGA-II) followed by the desirability function approach are the most suitable techniques for multi-objective optimization of turning of titanium grade-1 alloy under nanofluid MQL. These techniques provide a family of optimal solutions and one can have an option to select the process parameters from a set of optimal solutions. However, TOPSIS and Grey Relational analysis are lacking in providing a family of optimum solutions. However, they are suitable for obtaining quicker solutions due to less computational time especially for a limited range of the process parameters. This study suggests further investigations on the machinability of titanium grade-1 alloy under nanofluid MQL considering tool wear and surface integrity of the machined surface.

5. Conclusions

In the present study, the machining performance of CVD-coated TiCN-Al_2O_3 carbide inserts using vegetable oil-based nanofluid under minimum quantity lubrication is evaluated during turning of titanium grade-1 alloy. The resultant cutting force, machined surface roughness, and material removal rate (*MRR*) are measured varying the cutting speed, feed, depth of cut, and nanoparticles concentration in a base fluid. The nanofluid was prepared using coconut oil as a base fluid mixed with boron nitride (hBN) nanoparticles. The process parameters are optimized using the Desirability Function Approach (DFA), a Technique for Order of Preference by Similarity to Ideal Solution (TOPSIS), Grey Relational Analysis (GRA), and Non-dominated Sorting Genetic Algorithm (NSGA-II) for minimum *Fr*, minimum *Ra*, and maximum *MRR*. The following conclusions could be drawn from the present study.

- It has been observed that the selection of depth of cut and concentration of nanoparticles in the base fluid are more significant in obtaining lower resultant force as compared to feed. On the other hand, the depth of cut has been observed as significantly affecting the resultant force as compared to the concentration of nanoparticles in the base fluid.
- Surface roughness has been observed getting significantly affected with feed. However, the concentration of nanoparticles has been observed to have a negligible effect on the surface roughness. This study found that lower values of surface roughness and resultant force could be obtained with lower values of feed, depth of cut, and concentration of nanoparticles, and higher values of cutting speed. On the other hand, higher values for the material removal rate could be obtained with higher values of cutting speed, feed, and depth of cut.
- The optimized solutions obtained from different optimization techniques are observed in better agreement. The results show optimum performance at the higher cutting speed (120-125 m/min), higher depth of cut (0.7-0.75), lower feed (0.1-0.13 mm/rev), and lower concentration of nanoparticles (0.25-0.35%). Lowest values for resultant force and surface roughness of 387 N and 0.47 µm, respectively, and maximum *MRR* of 9375 mm^3/min could be obtained using the cutting speed, feed, depth of cut, and hBN nanoparticles concentration of 125 m/min, 0.1 mm/rev, 0.75 mm, and 0.3%, respectively.
- Little compromising on the surface roughness to a higher value of 0.83 µm with resultant force of 392 N, the higher *MRR* of 15000 mm^3/min could be obtained using cutting speed of 125 m/min, feed of 0.16 mm/rev, depth of cut of 0.75 mm, and nanoparticle concentration of 0.25%.
- This study finds that NSGA-II followed by the desirability function approach are better for multi-objective optimization of turning of titanium grade-1 alloy under nanofluid MQL in comparison to TOPSIS and GRA. TOPSIS and GRA has been observed in lacking in providing a family of optimal solutions. However, they are suitable for obtaining quicker solutions due to less computational time especially for a limited range of the process parameters.
- This study finds scope for further research on the machining of titanium alloys using hybrid nanofluids under MQL. A comprehensive study needs to be undertaken on parametric optimization of MQL machining of titanium alloys considering type, shape, size, the concentration of nanoparticles with the MQL parameters such as flow rate, nozzle orientation

angle, and air pressure

References

Aitken, R. J., Chaudhry, M. Q., Boxall, A. B. A., & Hull, M. (2006). Manufacture and use of nanomaterials: current status in the UK and global trends. Occupational medicine, 56(5), 300-306.

Anandan, V., Babu, M. N., Muthukrishnan, N., & Babu, M. D. (2020). Performance of silver nanofluids with minimum quantity lubrication in turning on titanium: a phase to green manufacturing. Journal of the Brazilian Society of Mechanical Sciences and Engineering, 42(4), 1-15.

Asadi, A., Saidi-Mehrabad, M., & Fathi Aghdam, F. (2019). A Two-Dimensional Warranty Model With Consideration Of Customer And Manufacturer Objectives Solved With Non-Dominated Sorting Genetic Algorithm. Journal Of Optimization In Industrial Engineering, 12(1), 15-22.

Boyer, R. R., & Briggs, R. D. (2005). The use of β titanium alloys in the aerospace industry. Journal of Materials Engineering and Performance, 14(6), 681-685.

Chinchanikar, S., Kore, S. S., & Hujare, P. (2021). A review on nanofluids in minimum quantity lubrication machining. Journal of Manufacturing Processes, 68, 56-70.

Chinchanikar, S., Bawangaonwala, H. M., Bokade, S., & Garode, S. (2020). Investigations on the Machining Performance using Solid Lubricant Mixed with Varying Proportions in Vegetable Oil during Hard Turning. In IOP Conference Series: Materials Science and Engineering (Vol. 810, No. 1, p. 012044). IOP Publishing.

Chinchanikar, S., & Choudhury, S. K. (2015). Machining of hardened steel—experimental investigations, performance modeling and cooling techniques: a review. International Journal of Machine Tools and Manufacture, 89, 95-109.

Chinchanikar, S., & Choudhury, S. K. (2013). Effect of work material hardness and cutting parameters on performance of coated carbide tool when turning hardened steel: An optimization approach. Measurement, 46(4), 1572-1584.

Das, S. K., Choi, S. U., & Patel, H. E. (2006). Heat transfer in nanofluids—a review. Heat transfer engineering, 27(10), 3-19.

Deb, K., Pratap, A., Agarwal, S., & Meyarivan, T. A. M. T. (2002). A fast and elitist multiobjective genetic algorithm: NSGA-II. IEEE transactions on evolutionary computation, 6(2), 182-197.

Dhar, N. R., Ahmed, M. T., & Islam, S. (2007). An experimental investigation on effect of minimum quantity lubrication in machining AISI 1040 steel. International Journal of Machine Tools and Manufacture, 47(5), 748-753.

Dhar, N. R., Kamruzzaman, M., & Ahmed, M. (2006). Effect of minimum quantity lubrication (MQL) on tool wear and surface roughness in turning AISI-4340 steel. Journal of materials processing technology, 172(2), 299-304.

Gaurav, G., Sharma, A., Dangayach, G. S., & Meena, M. L. (2020). Assessment of jojoba as a pure and nano-fluid base oil in minimum quantity lubrication (MQL) hard-turning of Ti–6Al–4V: A step towards sustainable machining. Journal of Cleaner Production, 272, 122553.

Gupta, M. K., Sood, P. K., & Sharma, V. S. (2016). Optimization of machining parameters and cutting fluids during nano-fluid based minimum quantity lubrication turning of titanium alloy by using evolutionary techniques. Journal of Cleaner Production, 135, 1276-1288.

Hegab, H., Umer, U., Deiab, I., & Kishawy, H. (2018). Performance evaluation of Ti-6Al-4V machining using nano-cutting fluids under minimum quantity lubrication. International Journal of Advanced Manufacturing Technology, 95, 4229–4241.

Jamil, M., He, N., Li, L., & Khan, A. M. (2020). Clean manufacturing of Ti-6Al-4V under CO2-snow and hybrid nanofluids. Procedia Manufacturing, 48, 131-140.

Jozić, S., Bajić, D., & Celent, L. (2015). Application of compressed cold air cooling: achieving multiple performance characteristics in end milling process. Journal of Cleaner Production, 100, 325-332.

Kalyon, A., Günay, M., & Özyürek, D. (2018). Application of grey relational analysis based on Taguchi method for optimizing machining parameters in hard turning of high chrome cast iron. Advances in Manufacturing, 6(4), 419-429.

Kang, M. C., Kim, K. H., Shin, S. H., Jang, S. H., Park, J. H., & Kim, C. (2008). Effect of the minimum quantity lubrication in high-speed end-milling of AISI D2 cold-worked die steel (62 HRC) by coated carbide tools. Surface and Coatings Technology, 202(22-23), 5621-5624.

Katta, S., & Chaitanya, R. S. (2018). Experimental Investigations of Graphene Nanoparticle-Based Cutting Fluid during Turning of Titanium Alloy (Grade 5) with Minimum Quantity Lubrication. Journal of Advanced Research in Manufacturing, Material Science & Metallurgical Engineering, 5(1&2), 22-30.

Kishawy, H. A., Dumitrescu, M., Ng, E. G., & Elbestawi, M. A. (2005). Effect of coolant strategy on tool performance, chip morphology and surface quality during high-speed machining of A356 aluminum alloy. International Journal of Machine Tools and Manufacture, 45(2), 219-227.

Khakzar Bafruei, M., Khatibi, S., & Rahmani, M. (2018). A Bi-Objective Airport Gate Scheduling with Controllable Processing Times Using Harmony Search and NSGA-II Algorithms. Journal of Optimization in Industrial Engineering, 11(1), 77-90.

Kosaraju, S., & Anne, V. G. (2013). Optimal machining conditions for turning Ti-6Al-4V using response surface methodology. Advances in Manufacturing, 1(4), 329-339.

Krishna, P. V., Srikant, R. R., & Rao, D. N. (2010). Experimental investigation on the performance of nanoboric acid suspensions in SAE-40 and coconut oil during turning of AISI 1040 steel. International Journal of machine Tools and manufacture, 50(10), 911-916.

Kumar, R., Sahoo, A. K., Mishra, P. C., & Das, R. K. (2018). Comparative study on machinability improvement in hard turning using coated and uncoated carbide inserts: part II modeling, multi-response optimization, tool life, and economic aspects. Advances in Manufacturing, 6(2), 155-175.

Kumar, T. A., Pradyumna, G., & Jahar, S. (2012). Investigation of thermal conductivity and viscosity of nanofluids. Journal of environmental research and development, 7(2).

Kumar, C. R. V., & Ramamoorthy, B. (2007). Performance of coated tools during hard turning under minimum fluid application. Journal of Materials Processing Technology, 185(1-3), 210-216.

Leppert, T. (2011). Effect of cooling and lubrication conditions on surface topography and turning process of C45 steel. International Journal of Machine Tools and Manufacture, 51(2), 120-126.

Li, N., Chen, Y. J., & Kong, D. D. (2019). Multi-response optimization of Ti-6Al-4V turning operations using Taguchi-based grey relational analysis coupled with kernel principal component analysis. Advances in Manufacturing, 7(2), 142-154.

Lin, J. L., & Tarng, Y. S. (1998). Optimization of the multi-response process by the Taguchi method with grey relational analysis. Journal of Grey system, 4(4), 355-370.

Liu, Z., An, Q., Xu, J., Chen, M., & Han, S. (2013). Wear performance of (nc-AlTiN)/(a-Si3N4) coating and (nc-AlCrN)/(a-Si3N4) coating in high-speed machining of titanium alloys under dry and minimum quantity lubrication (MQL) conditions. Wear, 305(1-2), 249-259.

Maadanpour Safari, F., Etebari, F., & Pourghader Chobar, A. (2021). Modelling and optimization of a tri-objective Transportation-Location-Routing Problem considering route reliability: using MOGWO, MOPSO, MOWCA and NSGA-II. Journal of Optimization in Industrial Engineering, 14(2), 99-114.

Maruda, R. W., Krolczyk, G. M., Michalski, M., Nieslony, P., & Wojciechowski, S. (2017). Structural and microhardness changes after turning of the AISI 1045 steel for minimum quantity cooling lubrication. Journal of Materials Engineering and Performance, 26(1), 431-438.

Rahmati, B., Sarhan, A. A., & Sayuti, M. (2014). Investigating the optimum molybdenum disulfide (MoS 2) nanolubrication parameters in CNC milling of AL6061-T6 alloy. The International Journal of Advanced Manufacturing Technology, 70(5-8), 1143-1155.

Rao, R. V. (2011). Overview. In Advanced Modeling and Optimization of Manufacturing Processes (pp. 1-54). Springer, London.

Sharma, A. K., Katiyar, J. K., Bhaumik, S., & Roy, S. (2019). Influence of alumina/MWCNT hybrid nanoparticle additives on tribological properties of lubricants in turning operations. Friction, 7(2), 6.

Sharma, A. K., Singh, R. K., Dixit, A. R., & Tiwari, A. K. (2017). Novel uses of alumina-MoS2 hybrid nanoparticle enriched cutting fluid in hard turning of AISI 304 steel. Journal of Manufacturing Processes, 30, 467-482.

Sharma, A. K., Tiwari, A. K., & Dixit, A. R. (2015). Progress of nanofluid application in machining: a review. Materials and Manufacturing Processes, 30(7), 813-828.

Singh, V., Sharma, A. K., Sahu, R. K., & Katiyar, J. K. (2021). Novel application of graphite-talc hybrid nanoparticle enriched cutting fluid in turning operation. Journal of Manufacturing Processes, 62, 378-387.

Varote, N., & Joshi, S. S. (2017). Microstructural analysis of machined surface integrity in drilling a titanium alloy. Journal of Materials Engineering and Performance, 26(9), 4391-4401.

This article can be cited:
Chinchanikar, S., Katiyar, J., Manav, O. (2022). Multi-objective Optimization of Turning of Titanium Alloy Under Minimum Quantity Lubrication. *Journal of Optimization in Industrial Engineering*, 15(1), 243-260.

http://www.qjie.ir/article_687008.html
DOI: 10.22094/joie.2021.1937743.1886